Mechanisms of peptide amphiphile internalization by SJSA-1 cells *in vitro*

Dimitris Missirlis[‡,*], **Htet Khant**[§], and **Matthew Tirrell**[‡]

Dimitris Missirlis: dimis@engineering.ucsb.edu; Htet Khant: htet.khant@gmail.com; Matthew Tirrell: tirrell@engineering.ucsb.edu

[‡]Department of Chemical Engineering and Materials Departments and Materials Research Laboratory, University of California, Santa Barbara, California 93106.

[§]National Center for Macromolecular Imaging, Department of Biochemistry and Molecular Biology, Baylor College of Medicine, One Baylor Plaza, Houston, TX 77030.

Abstract

Self-assembly of peptide amphiphiles into nanostructures makes them attractive for a variety of applications in drug and peptide delivery. We here report on the interactions of micelles composed of a palmitoylated, pro-apoptotic peptide derived from p53 tumor suppressor protein with a human cancer cell line. Characterization of self-assembly in aqueous buffered solutions revealed formation of elongated rod-like micelles above a critical micelle concentration. Our results however demonstrate that monomers instead of micelles are internalized, a finding which correlates with the dynamic nature of the assemblies and the non-covalent interactions that hold them together. Internalization is shown to occur via adsorption-mediated, energy-dependent pathways, resulting in accumulation of the material in endocytic vesicles. We conclude that palmitoylation of peptides is an efficient way to increase peptide permeability inside SJSA-1 cells and that increased micelle stability would be required for intact micelle internalization.

Synthetic peptides derived from human proteins, or identified via powerful new technologies, have emerged as potential therapeutics for various diseases, acting as signals, promoters or inhibitors of cellular functions. Frequently, their site of action is intracellular and therefore they are required to cross cell membranes in order to reach their target. Among the strategies explored in order to attain this goal, the one receiving the most attention is modification with peptide sequences that are able to translocate inside cells, widely referred to as cell penetrating peptides (CPPs)[1, 2]. A variety of different CPPs have been identified, ranging in activity and mechanism of action. An alternative strategy has been the covalent attachment of a hydrophobic tail onto the peptide of interest[3–6]. Borrowed from nature, where cells link hydrophobic moieties onto proteins to efficiently localize them on cellular membranes[7], this mechanism has proven a simple, yet effective way to transport peptides inside the cell and thus enhance their activity[8, 9]. Peptide amphiphiles or lipopeptides, as the resulting constructs are usually termed, have a higher affinity for lipid bilayers than the parent peptides[9, 10] and are able to insert into the cell membrane by virtue of their hydrophobic tail. Following this first step toward internalization, the subsequent uptake mechanism and the final destination of lipopeptides remain a subject of investigation. Attaching a hydrophobic tail onto a peptide additionally has implication on its biodistribution. Depending on the type of lipid tail, binding to certain biomolecules in vivo can be promoted in order to aid their transport to sites of interest[11] or act as a drug reservoir in the blood[12]. Moreover, lipopeptides exhibit improved stability against

CORRESPONDING AUTHOR FOOTNOTE, Dimitris Missirlis, Materials Research Laboratory, University of California, Santa Barbara, CA 93106, Tel. 805 893 7941, Fax. 805 893 8124.

degradation[13–15] in vitro as well as in vivo, although the reasons for this are yet to be determined.

From a materials science point of view, peptide amphiphiles have attracted attention due to their self-assembling capabilities and have been used as building blocks for novel materials in tissue engineering[16], cell encapsulation[17] and drug delivery[18]. Different aqueous solubilities of the peptide and lipid blocks promote segregation of the latter, leading to formation of supra-molecular structures[19, 20]. Peptides with various functionalities are thus presented on the surface of colloidal aggregates[21], fibrous meshes[16, 22] or two-dimensional flat surfaces[23, 24]. In our group, part of our effort is focused in the formulation of protein analogous micelles, capable of enhancing activity and circumventing peptide delivery obstacles[25]. Appropriate selection of hydrophobic tails and appropriate linkers between them and the functional peptide provides control over shape and size of the phase-separated aggregates and over activity retention, respectively. We envision preparing modular constructs, combining tumor-targeting peptides, internalization sequences and therapeutics for cancer treatment.

As an example of a pro-apoptotic signal we here selected a peptide derived from the binding site of tumor suppressor p53 to the MDM2 protein[26]. The 16-mer peptide from the N-terminus of p53 ($p53_{14–29}$) acts as an inhibitor of the p53-MDM2 interaction; competition by the peptide liberates wild-type p53, which is then rescued from degradation and nuclear export, allowing the cells to regain their apoptotic activity[27]. This protein-protein interaction is deregulated in approximately 50% of solid tumors and constitutes a therapeutically relevant target for pharmacological research[28, 29]. Among several approaches, small molecules, helix-mimetics and peptides have attracted most of the attention[30]. Specifically, peptide inhibitors based on the native sequence still face delivery problems; the peptide is not cell permeable and is prone to protease activity. In order for the peptide to reach its intracellular target synthesis of chimeras with a cell penetrating peptide[31, 32] as well as chemical stabilization with charge reversal[33] have been explored.

As an initial step toward development of an efficient delivery vehicle, we investigated the interactions of micelles composed solely of $p53_{14–29}$ peptide amphiphiles with cells in vitro. Our goal was to investigate the internalization process, the intracellular distribution of the peptide amphiphiles, and assess whether modifications through incorporation of cell-penetrating and/or endolysosomal-disrupting peptide amphiphiles was required to attain the desired localization. Although several studies have focused on internalization of acylated peptides, few have taken into consideration the aggregation properties of the peptide amphiphiles and how they influence uptake. We were interested in additionally studying how the self-assembled properties of the peptide amphiphiles influenced its association with a model cell line. We selected the SJSA-1 human, osteosarcoma cell line, which over-expresses MDM2 and possesses wild-type p53, making it prone to inhibition of the p53-MDM2 interaction for future cell viability studies. Our initial experiments showed that a significant amount of peptide was found inside the cells. We therefore undertook the task of dissecting the mechanism of uptake and discussing the potential of generally using peptide amphiphiles as a means to drive peptide internalization.

MATERIALS AND METHODS

Peptide Amphiphiles

The peptide derived from the N-terminus of p53 tumor suppressor protein ($p53_{14–29}$: LSQETFSDLWKLLPEN) was synthesized on a Rink amide resin (Novabiochem) using manual solid-phase synthesis and Fmoc-based chemistry[34]. A lysine was incorporated at the N-terminus of the sequence for fluorescent labeling at its ε-amine with 5,6-carboxytetramethylrhodamine (Fluka). Coupling of palmitic acid (Sigma) at the N-terminus

of the peptide was performed on the resin. Following cleavage from the resin, the peptides or peptide amphiphiles were purified using high pressure liquid chromatography (HPLC; Shimadzu Corporation) on a reverse-phase C4 column (Vydac), with gradients of acetonitrile (EMD chemicals, HPLC grade) in water containing 0.1% trifluoracetic acid (Sigma). Identity of the peptide amphiphiles was verified by electrospray ionization mass spectrometry and purity was determined using analytical HPLC on a reverse-phase C4 column (Vydac). Materials of purity greater than 95% were stored dry at −20°C until used. The chemical structure of the peptides/peptide amphiphiles is given in chart 1.

Self-assembly

Dissolution of lyophilized peptide amphiphiles in phosphate buffer saline (PBS) at room temperature did not result in reproducible self-assembly. In order to reproducibly prepare micelles the following protocol was used: peptide amphiphiles were dissolved in a 1:1 mixture of chloroform (BDH Chemicals) and methanol (BDH Chemicals) resulting in a clear solution. The solvents were then evaporated under N_2 flow. The residual films were dried under vacuum (> 2h) and hydrated in water or buffer at 60°C for 1h. After allowing cooling to room temperature, solutions were filtered with 0.45 um pore size syringe filters (Millipore). Mixed micelles were prepared by mixing the organic solutions at appropriate ratios prior to film formation.

Liposomes composed of egg phosphatidylcholine (egg PC; Avanti Polar Lipids) and the fluorescent lipid 1,2-Dioleoyl-sn-Glycero-3-Phospho-L-Serine-N-5-dimethylamino-1-Napthalenesulfonyl (Dansyl PS; Avanti Polar Lipids) were prepared using a similar protocol. Briefly, amphiphiles were dissolved in chloroform and the residual film after chloroform evaporation was dried under vacuum and hydrated for 1 hour at 70°C. The aqueous suspension of multilamellar vesicles was then extruded 10 times through a polycarbonate filter (100 nm nominal pore size, Millipore) at 37°C.

All aqueous solutions were stored at 4°C and used within a week of preparation.

Dynamic Light Scattering

Dynamic light scattering (DLS) was performed on a Brookhaven Instrument (model BI-DSI). Autocorrelation curves at different values of scattering vector, q, (angle range: 40° to 140°) were fitted using the cumulants method (quadratic fit) in order to obtain the average decay rate, Γ. The calculated diffusion coefficient exhibited a pronounced angle dependence indicating non-spherical geometry of micelles. The apparent diffusion coefficient was determined by extrapolation to q→0 from a linear fit of $\frac{\Gamma}{q^2}$ over q_2 Calculation of hydrodynamic diameters using the Stokes-Einstein equation resulted in values greater than 200 nm, thus excluding the formation of small spherical micelles. Assuming a rod-like micelle morphology with a cross-sectional diameter roughly equal to the length of two peptide amphiphiles (diameter=12 nm) and using the apparent diffusion coefficients, micelle length was approximated based on the model described by Tirado *et al.*[35].

Fluorescence spectroscopy

Fluorescence measurements were obtained using a Varian Cary Eclipse fluorescence spectrophotometer, with temperature set at 25°C. Steady state anisotropy was measured using manual polarization lenses and calculated using the following equation,

$$r = \frac{I_{VV} - I_{VH}I_{HV}/I_{HH}}{I_{VV} + 2I_{VH}I_{HV}/I_{HH}}$$

(1)

I_{VV}, I_{HH}, I_{VH} and I_{HV} are fluorescence intensities; the subscripts V and H stand for vertical and horizontal orientations of polarizers, respectively, with the first letter corresponding to the excited light and the second to the emitted light. The values of anisotropy presented here are averaged over a range of wavelengths (580–600 nm).

Kinetic measurements of fluorescence were performed to monitor micelle stability. A solution of RhoPA solution (110 ul) was placed in a 10 mm quartz cuvette and fluorescence was monitored at 585 nm. At a fixed time point (~2 min), a second solution (20 ul) was added so that the final concentration of RhoPA was 125 ug/ml (46.4 uM). Intensity was recorded for 20 min in real time. Then, steady state fluorescence and fluorescence anisotropy measurements were obtained.

A fluorescence method was used to determine apparent binding constants of RhoPA to 100 nm egg PC liposomes or bovine serum albumin (Sigma). Binding reactions can be written as:

$$RhoPA + Binder \leftrightarrow Binder-RhoPA \tag{2}$$

The apparent binding constant is then:

$$K_B = \frac{[Binder-RhoPA]}{[Binder][RhoPA]} \tag{3}$$

The total fluorescence intensity (I_{total}) stems from bound (I_b) and unbound (I_u) species:

$$I_{total} = I_u + I_b \tag{4}$$

At the experimental concentration range the fluorescence intensity of unbound RhoPA (RhoPA in micelles and free in solution) remained virtually constant with a value of $I_u = 32.0$. Fluorescence intensity of bound amphiphile was calculated based on a calibration curve of non-quenched RhoPep using equation:

$$I_b = 157.0 \times [Binder-RhoPA] \tag{5}$$

Combining equations 3, 4 and 5 we obtain:

$$I_{total} = I_u + 157.0 \times [RhoPA] \times [Binder] \times K_B \tag{6}$$

Therefore, plotting I_{total} versus ($157.0 \times [RhoPA] \times [Binder]$) should yield a straight line, with the slope equal to K_B.

Control experiments verified that liposomes and albumin did not exhibit fluorescence above baseline levels at the concentrations used here.

Liposomes composed of 95% mol egg PC and 5% mol dansyl PS were used to monitor förster resonance energy transfer (FRET) efficiency after binding of RhoPA or RhoPep to liposomes. Various amounts of RhoPA or RhoPep were added to a liposome suspension (0.1 mg/ml) to give ratios of tryptophan to dansyl of 0–10. The solution was excited at 280 nm (excitation of tryptophan) and emission was recorded from 300–550 nm (Tryptophan emission maximum is at 346 nm for RhoPA and 356 nm for Pep1 and dansyl emission maximum is at 520 nm)

In vitro Cell Studies

The human osteosarcoma SJSA-1 cell line (ATCC) was cultured as exponentially growing, sub-confluent monolayers in RPMI-1640 culture medium (ATCC), supplemented with 10% v/v calf bovine serum (ATCC) and 0.1% v/v Penicillin/Streptomycin (GIBCO). Cells were grown at 37°C, humidified atmosphere and 5% CO_2. For all *in vitro* studies SJSA-1 cells were seeded at a density of 15×10^3 cells/cm^2 and were allowed to attach on the surfaces overnight (12 h). Internalization of peptides and peptide amphiphiles was assessed using fluorescence microscopy and fluorescence activated cell-sorting (FACS) analysis.

For fluorescence microscopy imaging, cells were seeded in Lab-Tek chambered coverglass slides (Nalge Nunc) and incubated in presence of RhoPep or RhoPA for fixed periods of time. Next, medium was removed and adherent cells were washed three times with sterile filtered PBS (10 mM, pH 7.4). Cells were visualized in supplemented cell culture medium (cells retained their shape for a longer time when compared to visualization in PBS). Hoechst 33342 (Invitrogen) was added 10 minutes prior to washing in order to stain cell nuclei. A Nikon Eclipse TE-200 microscope equipped with a 40x and 100x objective and a 100W mercury arc lamp was used for fluorescence imaging. The acquired images were processed using ImageJ software with identical settings for peptides and peptide amphiphiles.

FACS analysis was performed in order to quantify internalization and investigate the effect of different culture conditions and inhibitors. Following incubation with peptides/peptide amphiphiles, cells were trypsinized and transferred to polycarbonate centrifuge tubes. A pellet was formed after centrifugation (5 min; 1500rpm) and supernatant was removed. Cells were resuspended in PBS and two more washing cycles were performed. Different inhibitors were used to block internalization pathways. In order to deplete cells of adenosine-5'-triphosphate (ATP), normal culture medium was replaced with medium containing 50 uM 2-D-deoxyglucose (Sigma) and 0.1% w/v sodium azide (Sigma) 30 minutes before addition of the formulations. Similarly, preincubation with culture medium containing 5mM methyl-β-cyclodextrin (MβCD; Sigma) was used to deplete membranes of cholesterol. For serum-free studies, cells were washed with serum-free media once before addition of peptide amphiphile in non-supplemented medium. For uptake studies at low temperature, cells and reagents were equilibrated at 4°C before peptide amphiphile addition and cells were washed twice with ice-cold PBS before centrifugation.

Cell suspensions after centrifugation were kept under ice until analyzed using a FACS Aria cytometer (BD Biosciences) equipped with a 488nm laser. Live cells were gated on forward and side scatter and a total of 10,000 events in the gated population were analyzed per sample.

RESULTS

We synthesized peptide p53$_{14-29}$ (Pep) derived from the MDM2-binding site of p53 tumor suppressor and modified it by linking palmitic (C_{16}) tail to its N-terminus (PA). Fluorescent analogs of the peptide (RhoPep) and peptide amphiphile (RhoPA) were also prepared by attaching rhodamine to a lysine incorporated for that purpose. The chemical structures of the molecules used in this study are presented in chart 1.

Physicochemical characterization of peptide amphiphile micelles

Above a certain concentration known as the critical micellar concentration (CMC), peptide amphiphiles self-assemble, shielding from water molecules their hydrophobic alkyl tails and exposing the peptides to the aqueous phase[34]. We determined the CMC at which assembly occurs using the pyrene solubilization method[36]: a value of 2.2 uM and 10.0 uM was calculated for PA and RhoPA, respectively (Supplementary figure S1).

Dynamic light scattering confirmed the existence of relatively monodisperse populations of scattering objects for solutions of PA, RhoPA and their mixtures in PBS. A pronounced angular dependence of Γ/q^2 indicated that the formed micelles were anisotropic, suggesting, therefore, a non-spherical geometry (Supplementary figure S2). Accordingly, apparent diffusion

coefficients that were estimated from $\lim\limits_{q\to 0}\dfrac{\Gamma}{q^2}$ corresponded to hydrodynamic diameters in the order of a few hundreds of nanometers, exceeding the predicted diameters for small spherical assemblies (Table 1). In order to determine micelle shape we performed cryo-TEM on a solution of PA above its CMC in PBS. Formation of elongated structures with high persistence length was observed (Supplementary figure S3). However, the low number of structures imaged was not sufficient for estimation of the micelle length, since cylindrical micelles are generally polydisperse in length. Based on the visual shape information, we selected a model for rod-like micelles to process our DLS data[35] and obtained approximate values for micelle length, assuming a diameter of 12 nm, which roughly corresponds to the length of 2 stretched peptide amphiphiles (Table 1). Average micelle length was found to be >1 um with increasing length as the ratio of labeled to non-labeled peptide amphiphile increased.

Incorporation of labeled monomers in mixed micelles rendered the micelles fluorescent. However, fluorescence intensity was not proportional to the amount of rhodamine present in the micelles (Figure 1). Self-quenching was evident above 3% mol of RhoPA, due to the close proximity of the neighboring rhodamine fluorophores. Accordingly, fluorescence from RhoPep was not quenched in the same concentration range, indicating that suppression of fluorescence is due to confinement, rather than an overall concentration effect (Figure 1). In micelles composed solely of RHoPA, fluorescence was highly suppressed and virtually independent of concentration in the range of 10–50 uM. As the ratio of labeled to non-labeled monomers decreased, an increase of steady state fluorescence was noted, suggesting dispersion of the labeled monomers inside the micelles. Anisotropy measurements further supported this finding: as the ratio of labeled amphiphiles increased, energy transfer between the closely positioned fluorophores led to a decrease in anisotropy (Table 1).

In vitro stability of peptide amphiphile micelles

Monomers are retained in the self-assembled structures through non-covalent, physical interactions. Equilibrium is established between monomers in micelles and unimers free in solution (which are present at a concentration equal to the CMC). We took advantage of rhodamine self-quenching to design an experimental setup that would allow us to monitor the kinetics and extent of mixing: an increase in rhodamine fluorescence intensity was attributed to mixing between micelles composed of RhoPA and PA, resulting in increase of spacing between the randomly distributed RhoPA monomers. Figure 2 shows a very rapid dequenching of fluorescence (< 10 sec) upon mixing of two different micelle solutions suggesting that equilibrium was reached in time periods that are not suitable for study with the experimental setup employed here. Following the initial jump in intensity, small variations were most likely due to rearrangement of the monomers within the mixed micelle (Figure 2A). The plateau value was in each case very close to that of mixed micelles obtained by mixing the monomers before hydration (Figure 2B). Moreover, anisotropy values were within 5 % of those for the preformed samples (data not shown).

The above findings provide evidence of rapid monomer mixing and formation of equilibrium structures. This led us to investigate micelle stability in presence of cell-membrane mimics and serum proteins. For the former we employed small, unilamellar, neutral liposomes, 140 nm in diameter, composed of egg PC, while for the latter we investigated the effect of addition of bovine serum albumin as well as the cell culture medium used in the cell studies, which was supplemented with calf bovine serum (10%) and antibiotics (1%).

In the presence of egg PC liposomes, an increase of total fluorescence was recorded as a fraction of peptide amphiphile rapidly partitioned into the lipid bilayer (Figure 3). Based on the assumptions that a) fluorescence intensity of RhoPA in micellar and unimer form is constant and b) fluorescence intensity of RhoPA bound to liposomes is not self-quenched, a binding constant of 28 M^{-1} was calculated (Figure 3B; see experimental section for analysis details). The first assumption was tested experimentally and the fluorescence intensity was found to be equal to 32.0±3.0 in the concentration range of 5–50 uM (Figure 1, black squares for 100% RhoPA). To test the validity of the second assumption we estimated the amount of peptide amphiphiles bound to the liposomes and found it to be less than 0.2 % mol: at this ratio the amphiphiles are not expected to interact with each other.

In order to gain additional proof that palmitoylated peptides were bound to liposomes by virtue of their hydrophobic tail, we monitored foerster resonance energy transfer (FRET) between W_{23} of the peptide and dansyl, which was incorporated at 5% mol on the surface of liposomes. Indeed, FRET was observed only for the peptide amphiphile confirming its association with the liposomes and excluding the possibility that there was a significant contribution from the peptide part (Figure 4).

Next, we monitored the effect of cell culture medium addition on micelle stability and observed the rapid dissociation of a fraction of micelles (Supplementary figure S4). Considering the complexity and high number of serum proteins, we decided to focus on the most abundant plasma protein, and a known binder of fatty acids, albumin. Using the same approach as for liposome binding we determined a binding constant of RhoPA to bovine serum albumin of $6.8 \times 10^3 \ M^{-1}$ (Supplementary figure S5). This value is nearly 200-fold greater than that calculated for liposomes and indicates the higher affinity of the peptide amphiphile towards albumin.

Cell Association of micelles with live SJSA1 cells

Covalent attachment of palmitic tail to rhodamine-labeled $p53_{14–29}$ rendered the peptide membrane-permeable for this cell line. Fluorescence microscopy of live SJSA-1 cells, following a 4 hour incubation with RhoPA micelles, revealed intracellular localization of the peptide amphiphile. In contrast, RhoPep levels inside live cells were not detectable using the same settings (Figure 5). The distribution of intracellular fluorescence was punctuate, suggesting that RhoPA was confined in vesicular, endocytic compartments (Figure 5 and supplementary figure S6).

In order to quantify uptake, flow cytometry was performed (Figure 6). Results confirmed microscopy observations. Peptide amphiphiles were internalized by SJSA1 cells to a greater extent than the fluorescent peptide, which exhibited fluorescence only slightly higher than the negative control. Virtually all cells took up RhoPA in a time dependent manner (Figure 6A). Significant fluorescence was detected as early as 10 minutes after RhoPA addition and increased over a period of 4 hours with kinetics indicative of an endocytotic mechanism (Figure 6B). Having in mind that micelles composed of 10% RhoPA and 90% PA exhibit several-fold higher fluorescence intensity in the aggregated state than those composed of 100% RhoPA, higher fluorescence levels were anticipated in case the micelles were internalized intact. However, incubation with these mixed micelles resulted in a marked decrease in mean fluorescence intensity per cell pointing to the conclusion that individual amphiphiles (unimers) rather than intact micelles enter the cells. Moreover, when cells were presented with the same amount of RhoPA, formulated in one-component micelles, equal uptake was recorded (Figure 6C).

We next aimed at elucidating the mechanism of uptake. As mentioned above fluorescent imaging and kinetic data suggest an endocytic mechanism. We incubated SJSA-1 cells at

different conditions (4°C, absence of serum) or in presence of chemical inhibitors (ATP depletion, cholesterol depletion) to gain insight on which internalization pathways are used (Figure 7). Uptake was abolished at 4°C, suggesting that the process of peptide amphiphile uptake requires energy consumption. However, at this temperature the properties of the membrane are significantly altered, making it difficult to discern between the effects of energy depletion and membrane rigidification. ATP depletion using a cocktail of sodium azide and 2-D-deoxyglucose, inhibited uptake approx. 70% confirming that energy is indeed required. Serum proteins and cholesterol were also found to influence uptake, albeit to a lesser extent: in the absence of serum an inhibition of approximately 20% was noted, while cholesterol depletion by MβCD caused a 25% reduction in uptake.

DISCUSSION

In the present report we demonstrate that palmitoylation of p53$_{14-29}$ peptide enhances its uptake into SJSA-1 cells and investigate the mechanisms through which internalization occurs. A major obstacle for efficient inhibition of the p53-MDM2 interaction *in vivo* using this peptide is intracellular delivery. Although more potent inhibitors identified by phage display[37, 38] and structural considerations[39] have been identified, we here chose to work with the native sequence derived from the MDM2-binding region of wild-type p53, in order to validate our approach. Internalization of this peptide after linkage to a cell-penetrating agent caused cell death. We initially pursued palmitoylation as a means to drive self-assembly of the peptide amphiphiles into micelles; later, combination with different peptide amphiphiles containing cell penetrating motifs and targeting moieties would result in mixed micelles able to efficiently deliver the apoptotic peptide in aggregated form *in vivo*. In this way the essential targeting and delivery functionalities as well as the therapeutic would be combined in *one* modular construct, with potential for multivalent peptide presenation. Our results showed that a significant amount of peptide amphiphile accumulated inside SJSA-1 osteosarcoma cells without the use of additional peptides. We therefore focused on cellular uptake and intracellular localization while considering the aggregation state of the peptide amphiphiles; a thorough examination of the self-assembly process will be reported elsewhere.

Several studies have proposed acylation as a means to promote cell penetration but have not discussed the self-assembly properties of the resulting amphiphiles[3–5, 13, 40, 41] The observation that acylated peptides induce robust immune responses in the absence of adjuvants sparked an interest in lipopeptide interactions with antigen-presenting cells, which established the enhancement of uptake following attachment of lipid tails[13, 40, 42]. Analogous results have been obtained for various cell lines and peptides suggesting that acylation could be a general method for the creation of cell-permeable peptide constructs. Nelson et al. recently compared the use of myristoylation to the use of the cell penetrating peptide TAT in two different cell lines and argued that the former is a more general methodology to introduce peptide inside cells[3]. In agreement with these studies, we here showed that p53$_{14-29}$ peptide amphiphiles were internalized into SJSA-1 cells at a greater extent compared to unmodified peptide. In contrast, however, to previous reports we placed emphasis on the self-association of the acylated peptides in order to interpret our findings and dissect the internalization mechanisms. In PBS solutions, the peptide amphiphiles form long, rod-like micelles above a critical micelle concentration. Since our *in vitro* experiments were performed at concentrations much higher than the CMC, the question arose as to which species is internalized, whether it is monomeric peptide amphiphiles or micelles. Based on a demonstrated self-quenching of fluorescence in the aggregated state, we were able to show that cell-associated fluorescence was proportional to the amount of labeled monomer rather than the fluorescent properties of the micelles. This finding point to the conclusion that intracellular fluorescence does not stem from internalized micelles but instead from monomers.

The non-covalent nature of interactions between monomers in the aggregated state prompted us to investigated micelle stability in presence of proteins and cell-membrane mimetics. Initially, the kinetics of exchange between monomers in solution (unimers) and the aggregated state was probed. We found that for single-tailed peptide amphiphiles monomer mixing is very rapid with a complete reorganization between two different micelle populations occurring within a few seconds (<10 s). An implication of this finding was that monomer binding to biomolecules or partitioning into membranes would lead to a shift in equilibrium and result in micelle disassembly. Indeed, rapid association of the peptide amphiphiles with phospholipid bilayers or albumin resulted in concomitant disassembly of a fraction of the micelle population. It is well-established experimentally[10, 43] and predicted computationally[44, 45], that fatty acids and lipopeptides insert into phospholipid bilayers. Our finding that single-tailed peptide amphiphiles associate with egg PC lipid membranes (intended to imitate cell membranes) was therefore not surprising. Unlike fatty acids however, peptide amphiphiles are not expected to cross membranes passively by the flip-flop mechanism due to the large and ionized peptide headgroup. An affinity for cell membranes should help localize free peptide amphiphiles on the cell surface, which is the first step of their subsequent internalization. Peptide amphiphiles also bound to albumin, with higher affinity than for lipid membranes. Albumin is the most abundant plasma protein (0.6mM concentration in plasma) and directly binds fatty acids regulating their blood concentration and transporting them throughout the body[46]. Presumably, binding of peptide amphiphiles with fatty acid tails occurs in a similar manner. This effect has been the basis of the development of lipidated insulin, now in the market for the treatment of diabetes[12, 47].

Based on previous studies and as shown also here, the unmodified fluorescent peptide is not cell permeable. A low amount is taken up, presumably by fluid-phase pinocytosis. This finding excludes the possibility that uptake is mediated through attachment of the fluorophore. We were therefore interested in understanding how attachment of a hydrophobic tail facilitates uptake and through which pathways the peptide amphiphiles are internalized. Having shown an affinity to albumin we hypothesized that uptake might be mediated via the formation of a protein-amphiphile complex in the cell culture medium. However, in the absence of serum, uptake decreased only slightly suggesting that serum proteins were not required for the most part. The small increase in uptake in their presence might be due to albumin mediated delivery to the cell membrane through binding to receptors as has been shown for albumin and fatty acid uptake in adipocytes[48]. Alternatively, an equilibrium shift between aggregated and monomeric states by protein-mediated micelle breakup could be responsible for the observed uptake increase..

Fluorescence microscopy images revealed a punctuate pattern of fluorescence, indicative of distribution in intracellular vesicular compartments. Our images resemble those from reports of lipopeptide entry into live antigen presenting cells[13], and of sterol-conjugated peptides in HeLa cells[9]. Several groups have argued that a fraction of peptide amphiphiles is able to reach the cytoplasm [6, 13, 40, 42, 49]. Although we cannot exclude this possibility, the amount of peptide amphiphile in the cytoplasm in our studies would be minimal, below the detection levels of our experimental setup. Moreover, conclusions that were based on observations of fixed cells[40, 42, 49] should be viewed with caution considering the potential of artifactual staining as has previously been demonstrated[50]. Vesicle formation after uptake is a common way cells manage to pick up extacellular material; the plasma membrane invaginates via help of proteins and specific lipid compositions carrying membrane-bound species and surrounding fluid inside cells. The process often requires energy. The observations that uptake was a) abolished at 4 degrees and b) inhibited ~70% when cells were depleted of ATP, point to energy-dependent endocytosis as the main uptake mechanism. Cholesterol depletion inhibited to a low but significant extent (30%) uptake. Removal of cholesterol from the plasma membrane disrupts caveolae formation and is required for clathrin-coated pit budding[51, 52]. The low

inhibition recorded in presence of methyl-β-cyclodextrin suggests that caveolae- and clathrin-independent mechanisms are at play. Moreover, the kinetics of uptake are suggestive of an endocytotic mechanism rather than direct passive diffusion through the plasma membrane.

Taken together our data points towards internalization of peptide amphiphiles through energy-dependent endocytosis, through caveolae- and clathrin-independent pathways. The hydrophobic segment facilitates initial attachment to the membrane; it remains unclear whether insertion in the membrane occurs in specialized areas of the membrane (lipid rafts) or is non-specific. Also, it remains to be investigated whether the peptide amphiphile promotes formation of invaginations on the cell surface or is passively localized in them during normal cell internalization processes. Our results suggest that once internalized the peptide remains trapped inside endosomal vesicles, which would prevent it of reaching its target, MDM2. Endosomal escape has been shown to be the rate limiting step for the CPP-assisted delivery of peptides and strategies to disrupt endosomes using appropriate agents have been developed[32, 53, 54] and merit further investigation.

Our initial view of delivering intact micelles composed of single-tailed amphiphiles *in vivo* is therefore challenged; the high blood levels of albumin and the presence of cells in blood and blood vessels will rapidly adsorb the peptide amphiphiles and cause micelles to disassemble. To deliver intact micelles, presenting tumor-targeting peptides as well as pro-apoptotic $p53_{14-29}$, strategies that enhance monomer association and hence stability are required. Double-tailed peptide amphiphile micelles have already been successfully delivered *in vivo*[55]. Polymerizing peptide amphiphiles prepared by use of diacetylene acid tails is another way to prepare robust delivery vehicles[56]. Nevertheless, our findings substantiate the use of lipid-modification of $p53_{14-29}$ as an efficient way to enter cells via adsorptive-mediated endocytosis and point to the possibility of this being a general methodology for preparing cell-permeable peptides.

Supplementary Material

Refer to Web version on PubMed Central for supplementary material.

Acknowledgments

ABBREVIATIONS

CPPs, Cell Penetrating Peptides
MDM2, Murine Double Minute 2
HPLC, High Pressure Liquid Chromatography
PBS, Phosphate Buffer Saline
PC, Phosphatidylcholine
Dansyl PS, 1,2-Dioleoyl-sn-Glycero-3-Phospho-L-Serine-N-5-dimethylamino-1-Napthalenesulfonyl
DLS, Dynamic Light Scattering
TEM, Transmission Electron Microscopy
FRET, Förster Resonance Energy Transfer
FACS, Fluorescence Activated Cell Sorting
ATP, Adenosine-5'-Triphosphate
MβCD, Methyl-β-Cyclodextrin
CMC, Critical Micelle Concentration

BSA, Bovine Serum Albumin

REFERENCES

1. Fischer PM. Cellular uptake mechanisms and potential therapeutic utility of peptidic cell delivery vectors: progress 2001–2006. Med Res Rev 2007;27(6):755–795. [PubMed: 17019680]

2. Foerg C, Merkle HP. On the biomedical promise of cell penetrating peptides: limits versus prospects. J Pharm Sci 2008;97(1):144–162. [PubMed: 17763452]

3. Nelson AR, Borland L, Allbritton NL, Sims CE. Myristoyl-based transport of peptides into living cells. Biochemistry 2007;46(51):14771–14781. [PubMed: 18044965]

4. Ensenat-Waser R, Martin F, Barahona F, Vazquez J, Soria B, Reig JA. Direct visualization by confocal fluorescent microscopy of the permeation of myristoylated peptides through the cell membrane. IUBMB Life 2002;54(1):33–36. [PubMed: 12387573]

5. Carrigan CN, Imperiali B. The engineering of membrane-permeable peptides. Anal Biochem 2005;341 (2):290–298. [PubMed: 15907875]

6. Stephens G, O'Luanaigh N, Reilly D, Harriott P, Walker B, Fitzgerald D, Moran N. A sequence within the cytoplasmic tail of GpIIb independently activates platelet aggregation and thromboxane synthesis. J Biol Chem 1998;273(32):20317–20322. [PubMed: 9685382]

7. Resh MD. Trafficking and signaling by fatty-acylated and prenylated proteins. Nat Chem Biol 2006;2 (11):584–590. [PubMed: 17051234]

8. Eichholtz T, de Bont DB, de Widt J, Liskamp RM, Ploegh HL. A myristoylated pseudosubstrate peptide, a novel protein kinase C inhibitor. J Biol Chem 1993;268(3):1982–1986. [PubMed: 8420972]

9. Rajendran L, Schneider A, Schlechtingen G, Weidlich S, Ries J, Braxmeier T, Schwille P, Schulz JB, Schroeder C, Simons M, Jennings G, Knolker HJ, Simons K. Efficient inhibition of the Alzheimer's disease beta-secretase by membrane targeting. Science 2008;320(5875):520–523. [PubMed: 18436784]

10. Peitzsch RM, McLaughlin S. Binding of acylated peptides and fatty acids to phospholipid vesicles: pertinence to myristoylated proteins. Biochemistry 1993;32(39):10436–10443. [PubMed: 8399188]

11. Mims MP, Darnule AT, Tovar RW, Pownall HJ, Sparrow DA, Sparrow JT, Via DP, Smith LC. A nonexchangeable apolipoprotein E peptide that mediates binding to the low density lipoprotein receptor. J Biol Chem 1994;269(32):20539–20547. [PubMed: 8051153]

12. Havelund S, Plum A, Ribel U, Jonassen I, Volund A, Markussen J, Kurtzhals P. The mechanism of protraction of insulin detemir, a long-acting, acylated analog of human insulin. Pharm Res 2004;21 (8):1498–1504. [PubMed: 15359587]

13. Andrieu M, Loing E, Desoutter JF, Connan F, Choppin J, Gras-Masse H, Hanau D, Dautry-Varsat A, Guillet JG, Hosmalin A. Endocytosis of an HIV-derived lipopeptide into human dendritic cells followed by class I-restricted CD8(+) T lymphocyte activation. Eur J Immunol 2000;30(11):3256–3265. [PubMed: 11093141]

14. Toth I, Flinn N, Hillery A, Gibbons WA, Artursson P. Lipidic Conjugates of Luteinizing-Hormone-Releasing Hormone (Lhrh)+ and Thyrotropin-Releasing-Hormone (Trh)+ That Release and Protect the Native Hormones in Homogenates of Human Intestinal Epithelial (Caco-2) Cells. International Journal of Pharmaceutics 1994;105(3):241–247.

15. Dasgupta P, Mukherjee R. Lipophilization of somatostatin analog RC-160 with long chain fatty acid improves its antiproliferative and antiangiogenic activity in vitro. Br J Pharmacol 2000;129(1):101–109. [PubMed: 10694208]

16. Silva GA, Czeisler C, Niece KL, Beniash E, Harrington DA, Kessler JA, Stupp SI. Selective differentiation of neural progenitor cells by high-epitope density nanofibers. Science 2004;303 (5662):1352–1355. [PubMed: 14739465]

17. Capito RM, Azevedo HS, Velichko YS, Mata A, Stupp SI. Self-assembly of large and small molecules into hierarchically ordered sacs and membranes. Science 2008;319(5871):1812–1816. [PubMed: 18369143]

18. Rezler EM, Khan DR, Lauer-Fields J, Cudic M, Baronas-Lowell D, Fields GB. Targeted drug delivery utilizing protein-like molecular architecture. J Am Chem Soc 2007;129(16):4961–4972. [PubMed: 17397150]

19. Cavalli S, Kros A. Scope and applications of amphiphilic alkyl- and lipopeptides. Advanced Materials 2008;20(3):627–631.

20. Lowik DW, van Hest JC. Peptide based amphiphiles. Chem Soc Rev 2004;33(4):234–245. [PubMed: 15103405]

21. Boato F, Thomas RM, Ghasparian A, Freund-Renard A, Moehle K, Robinson JA. Synthetic virus-like particles from self-assembling coiled-coil lipopeptides and their use in antigen display to the immune system. Angew Chem Int Ed Engl 2007;46(47):9015–9018. [PubMed: 17935102]

22. Rajangam K, Behanna HA, Hui MJ, Han X, Hulvat JF, Lomasney JW, Stupp SI. Heparin binding nanostructures to promote growth of blood vessels. Nano Lett 2006;6(9):2086–2090. [PubMed: 16968030]

23. Biesalski MA, Knaebel A, Tu R, Tirrell M. Cell adhesion on a polymerized peptide-mphiphile monolayer. Biomaterials 2006;27(8):1259–1269. [PubMed: 16157369]

24. Stroumpoulis D, Zhang H, Rubalcava L, Gliem J, Tirrell M. Cell adhesion and growth to Peptide-patterned supported lipid membranes. Langmuir 2007;23(7):3849–3856. [PubMed: 17335250]

25. Chu-Kung AF, Bozzelli KN, Lockwood NA, Haseman JR, Mayo KH, Tirrell MV. Promotion of peptide antimicrobial activity by fatty acid conjugation. Bioconjug Chem 2004;15(3):530–535. [PubMed: 15149180]

26. Kussie PH, Gorina S, Marechal V, Elenbaas B, Moreau J, Levine AJ, Pavletich NP. Structure of the MDM2 oncoprotein bound to the p53 tumor suppressor transactivation domain. Science 1996;274 (5289):948–953. [PubMed: 8875929]

27. Kastantin M, Ananthanarayanan B, Lin B, Ressl J, Black M, Tirrell M. Increase of fluorescence anisotropy upon self-assembly in headgroup-labeled surfactants. Macromol Biosci 2007;7(2):189–194. [PubMed: 17295406]

28. Chene P. Inhibiting the p53-MDM2 interaction: an important target for cancer therapy. Nat Rev Cancer 2003;3(2):102–109. [PubMed: 12563309]

29. Vassilev LT. MDM2 inhibitors for cancer therapy. Trends Mol Med 2007;13(1):23–31. [PubMed: 17126603]

30. Murray JK, Gellman SH. Targeting protein-protein interactions: Lessons from p53/MDM2. Biopolymers 2007;88(5):657–686. [PubMed: 17427181]

31. Harbour JW, Worley L, Ma D, Cohen M. Transducible peptide therapy for uveal melanoma and retinoblastoma. Arch Ophthalmol 2002;120(10):1341–1346. [PubMed: 12365913]

32. Yoshikawa T, Sugita T, Mukai Y, Yamanada N, Nagano K, Nabeshi H, Yoshioka Y, Nakagawa S, Abe Y, Kamada H, Tsunoda S, Tsutsumi Y. Organelle-targeted delivery of biological macromolecules using the protein transduction domain: potential applications for Peptide aptamer delivery into the nucleus. J Mol Biol 2008;380(5):777–782. [PubMed: 18571668]

33. Bernal F, Tyler AF, Korsmeyer SJ, Walensky LD, Verdine GL. Reactivation of the p53 Tumor Suppressor Pathway by a Stapled p53 Peptide. J Am Chem Soc 2007;129(9):2456–2457. [PubMed: 17284038]

34. Tu RS, Tirrell M. Bottom-up design of biomimetic assemblies. Adv Drug Deliv Rev 2004;56(11): 1537–1563. [PubMed: 15350288]

35. Tirado MM, Martinez CL, Delatorre JG. Comparison of Theories for the Translational and Rotational Diffusion-Coefficients of Rod-Like Macromolecules - Application to Short DNA Fragments. Journal of Chemical Physics 1984;81(4):2047–2052.

36. Astafieva I, Zhong XF, Eisenberg A. Critical Micellization Phenomena in Block Polyelectrolyte Solutions. Macromolecules 1993;26(26):7339–7352.

37. Bottger A, Bottger V, Garcia-Echeverria C, Chene P, Hochkeppel HK, Sampson W, Ang K, Howard SF, Picksley SM, Lane DP. Molecular characterization of the hdm2-p53 interaction. J Mol Biol 1997;269(5):744–756. [PubMed: 9223638]

38. Hu B, Gilkes DM, Chen J. Efficient p53 Activation and Apoptosis by Simultaneous Disruption of Binding to MDM2 and MDMX. Cancer Res 2007;67(18):8810–8817. [PubMed: 17875722]

39. Garcia-Echeverria C, Chene P, Blommers MJ, Furet P. Discovery of potent antagonists of the interaction between human double minute 2 and tumor suppressor p53. J Med Chem 2000;43(17): 3205–3208. [PubMed: 10966738]

40. Pfender NA, Grosch S, Roussel G, Koch M, Trifilieff E, Greer JM. Route of uptake of palmitoylated encephalitogenic peptides of myelin proteolipid protein by antigen-presenting cells: importance of the type of bond between lipid chain and peptide and relevance to autoimmunity. J Immunol 2008;180 (3):1398–1404. [PubMed: 18209034]

41. Pham W, Kircher MF, Weissleder R, Tung CH. Enhancing membrane permeability by fatty acylation of oligoarginine peptides. Chembiochem 2004;5(8):1148–1151. [PubMed: 15300843]

42. Zhu X, Ramos TV, Gras-Masse H, Kaplan BE, BenMohamed L. Lipopeptide epitopes extended by an Nepsilon-palmitoyl-lysine moiety increase uptake and maturation of dendritic cells through a Toll-like receptor-2 pathway and trigger a Th1-dependent protective immunity. Eur J Immunol 2004;34 (11):3102–3114. [PubMed: 15368273]

43. D'Errico G, D'Ursi AM, Marsh D. Interaction of a peptide derived from glycoprotein gp36 of feline immunodeficiency virus and its lipoylated analogue with phospholipid membranes. Biochemistry 2008;47(19):5317–5327. [PubMed: 18419135]

44. Jensen MO, Mouritsen OG, Peters GH. Simulations of a membrane-anchored peptide: structure, dynamics, and influence on bilayer properties. Biophys J 2004;86(6):3556–3575. [PubMed: 15189854]

45. Gorfe AA, Pellarin R, Caflisch A. Membrane localization and flexibility of a lipidated ras peptide studied by molecular dynamics simulations. J Am Chem Soc 2004;126(46):15277–15286. [PubMed: 15548025]

46. Kratz F. Albumin as a drug carrier: Design of prodrugs, drug conjugates and nanoparticles. J Control Release 2008;132(3):171–183. [PubMed: 18582981]

47. Kurtzhals P, Havelund S, Jonassen I, Kiehr B, Larsen UD, Ribel U, Markussen J. Albumin binding of insulins acylated with fatty acids: characterization of the ligand-protein interaction and correlation between binding affinity and timing of the insulin effect in vivo. Biochem J 1995;312(Pt 3):725–731. [PubMed: 8554512]

48. Trigatti BL, Gerber GE. A direct role for serum albumin in the cellular uptake of long-chain fatty acids. Biochem J 1995;308(Pt 1):155–159. [PubMed: 7755560]

49. Thiam K, Loing E, Zoukhri D, Rommens C, Hodges R, Dartt D, Verwaerde C, Auriault C, Gras-Masse H, Sergheraert C. Direct evidence of cytoplasmic delivery of PKC-alpha, - epsilon and -zeta pseudosubstrate lipopeptides: study of their implication in the induction of apoptosis. FEBS Lett 1999;459(3):285–290. [PubMed: 10526151]

50. Richard JP, Melikov K, Vives E, Ramos C, Verbeure B, Gait MJ, Chernomordik LV, Lebleu B. Cell-penetrating peptides. A reevaluation of the mechanism of cellular uptake. J Biol Chem 2003;278(1):585–590. [PubMed: 12411431]

51. Subtil A, Gaidarov I, Kobylarz K, Lampson MA, Keen JH, McGraw TE. Acute cholesterol depletion inhibits clathrin-coated pit budding. Proc Natl Acad Sci U S A 1999;96(12):6775–6780. [PubMed: 10359788]

52. Rodal SK, Skretting G, Garred O, Vilhardt F, van Deurs B, Sandvig K. Extraction of cholesterol with methyl-beta-cyclodextrin perturbs formation of clathrin-coated endocytic vesicles. Mol Biol Cell 1999;10(4):961–974. [PubMed: 10198050]

53. El-Sayed A, Khalil IA, Kogure K, Futaki S, Harashima H. Octaarginine- and octalysine-modified nanoparticles have different modes of endosomal escape. J Biol Chem 2008;283(34):23450–23461. [PubMed: 18550548]

54. Caron NJ, Quenneville SP, Tremblay JP. Endosome disruption enhances the functional nuclear delivery of Tat-fusion proteins. Biochem Biophys Res Commun 2004;319(1):12–20. [PubMed: 15158435]

55. Karmali PP, Kotamraju VR, Kastantin M, Black M, Missirlis D, Tirrell M, Ruoslahti E. Targeting of albumin-embedded paclitaxel nanoparticles to tumors. Nanomedicine. 2008in press

56. Biesalski M, Tu R, Tirrell MV. Polymerized vesicles containing molecular recognition sites. Langmuir 2005;21(13):5663–5666. [PubMed: 15952804]
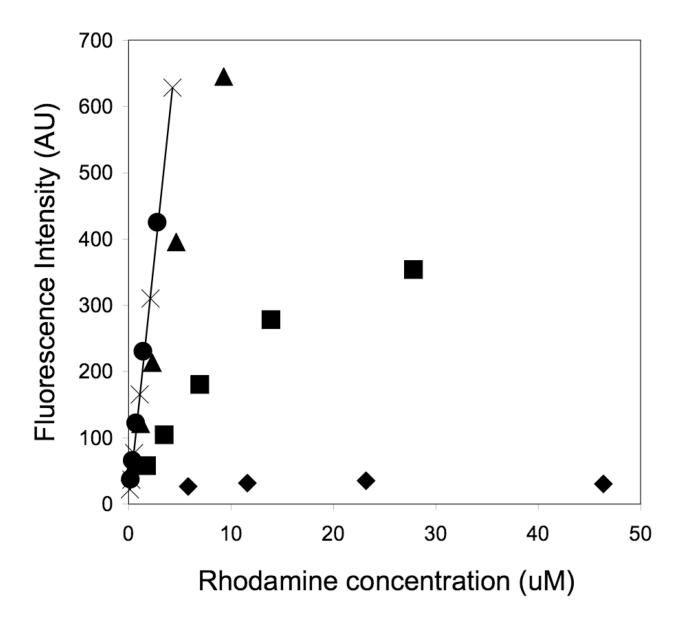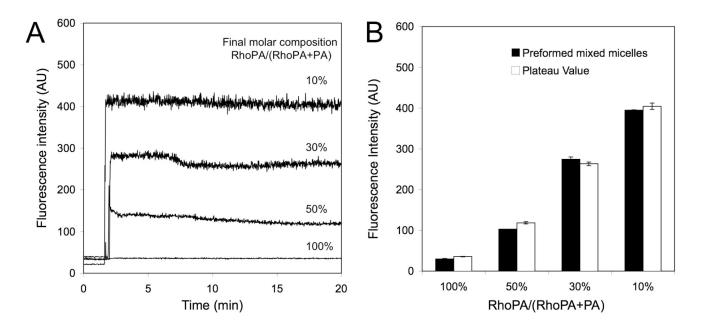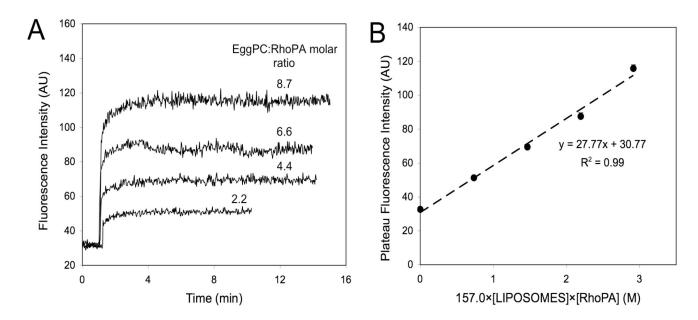
Figure 1.
Fluorescence intensity as a function of rhodamine concentration for the peptide and peptide amphiphiles micelles of different compositions. Self-quenching is evident for micelles composed of 100% mol RhoPA (◆), 30% mol RhoPA (■) and 10% mol RhoPA (▲) but not for micelles containing 3% mol RhoPA (●). The solid line represents the calibration curve for unquenched rhodamine-labeled peptide, RhoPep (×). All measurements were performed in PBS, at 25°C (excitation: 560 nm, emission: 580 nm).

Figure 2.
(A) Kinetics of rhodamine fluorescence intensity increase after adding a 100% PA micelle solution to a 100% RhoPA micelle solution at different ratios (final total monomer concentration was the same in all cases). (B) Comparison of plateau intensity values from (A) with values obtained from preformed mixed samples of same composition indicating that equilibrium is reached. All measurements were performed in PBS, at 25°C (excitation: 560nm; emission: 580nm).

Figure 3.
Determination of RhoPA binding constant to egg PC liposomes. (A) Kinetic profiles of rhodamine de-quenching upon addition of liposome suspensions. (B) Calculation of binding constant from the slope of the linear fit (see text for details).
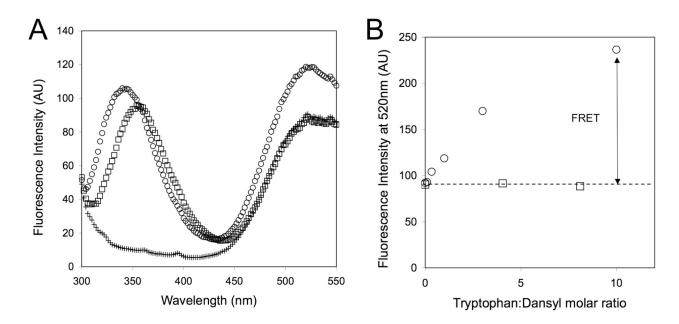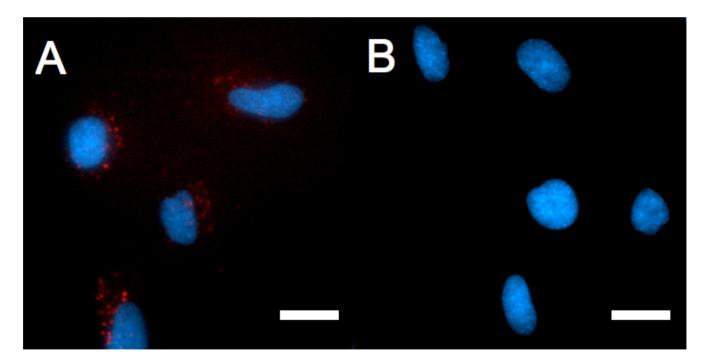
Figure 4.
Förster resonance energy transfer (FRET) between tryptophan (W_{23}) of the peptide/peptide amphiphile and dansyl fluorophores immobilized on the surface of liposomes. (A) Fluorescence spectra showing both tryptophan and dansyl emission upon excitation at 280nm for suspensions of liposomes containing 5% dansyl PS in the presence of PA (○), Pep (□) or in their absence (+) (B) Graph showing efficient FRET from tryptophan to dansyl in the presence of the peptide amphiphile but not of the peptide.

Figure 5.
Fluorescence microscopy images of live SJSA1 cells showing internalization of RhoPA (A) and RhoPep (B). Rhodamine-labeled peptides/peptide amphiphiles (red) were incubated 4 hours in presence of cells at a concentration of 100 ug/ml. Nuclei are stained by Hoechst 33342 (blue). Scale bar: 20 um.
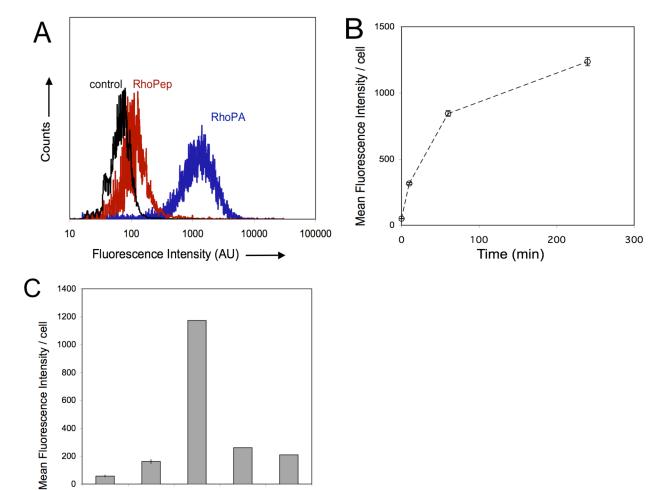
Figure 6.
Quantification of peptide/peptide amphiphile association with SJSA-1 cells by flow cytometry. (A) Histograms of SJSA-1 association after 4 hour incubation with 100ug/ml RhoPA (blue line), 100 ug/ml RhoPep (red line) or control cells (black line). (B) Kinetics of RhoPA (100 ug/ml) internalization. Mean and standard deviations of 3 samples are shown. (C) Mean intensity per cell after 4 hour incubation with RhoPep and RhoPA micelles of difference concentrations and compositions. Mean and standard deviation of 2 independent experiments are presented (each condition in an experiment is performed in triplicate).
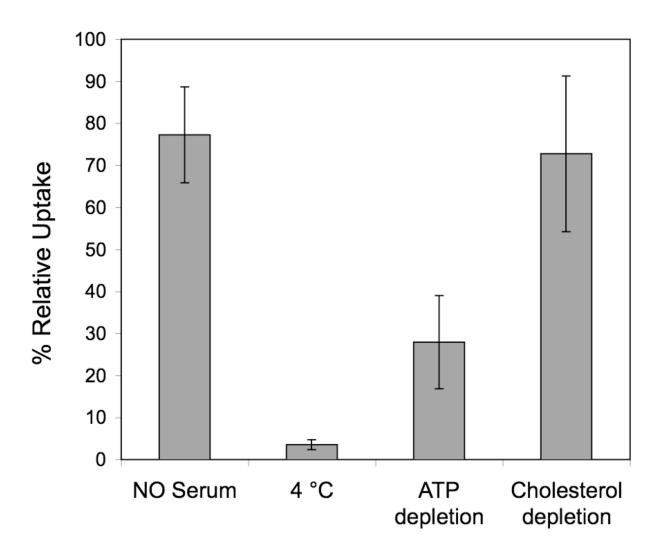
Figure 7.
Effect of different incubation conditions and presence of inhibitors on uptake of RhoPA by SJSA1 cells. Results are expressed as % uptake relative to standard incubation conditions. Mean and standard deviation of 2 independent experiments are presented (each condition in an experiment is performed in triplicate).

Chart 1.
Structure of peptides and peptide amphiphiles used in the present study

Table 1

Effect of micelle composition on micelle diffusion coefficient, hydrodynamic diameter, length and rhodamine fluorescence anisotropy

RhoPA/(RhoPA+PA) (% mol)	Apparent Diffusion Coefficient (10^{-8} cm^2/s)	Hydrodynamic diameter (nm)	Micelle Length (um)	Rhodamine Anisotropy
0	1.53	314	1.4	-
3	1.32	372	1.7	0.32
10	1.22	401	2.0	0.32
30	1.12	437	2.2	0.26
50	-	-	-	0.20
100	0.78	628	3.4	0.12